Received: 28 June 2022 | Revised: 15 September 2022 | Accepted: 23 October 2022

DOI: 10.1002/hyp.14749

RESEARCH ARTICLE

WILEY

The mechanics of diurnal thermal stratification in river pools: Implications for water management and species conservation

Todd H. Buxton[1] | Yong G. Lai[2] | Nicholas A. Som[3,4] | Eric Peterson[1] | Ben Abban[2]

[1]Trinity River Restoration Program, U.S. Bureau of Reclamation, Weaverville, California, USA

[2]Technical Service Centre, U.S. Bureau of Reclamation, Denver, Colorado, USA

[3]U.S. Fish and Wildlife Service, Arcata Field Office, Arcata, California, USA

[4]Department of Fisheries Biology, California Polytechnic University, Humboldt, Arcata, California, USA

Correspondence
Todd H. Buxton, Trinity River Restoration Program, 1313 South Main Street, Weaverville, CA 96093, USA.
Email: tbuxton@usbr.gov

Funding information
Trinity River Restoration Program

Abstract

We examined conditions that form or prevent thermal stratification in river pools using field measurements, statistical modelling, and three-dimensional (3D) computational fluid dynamics (CFD) modelling. Our motivation is to identify variables that control stratification for exploitation to enhance or prevent thermal gradients as needed to benefit species in rivers. One study pool (UT) is located above water storage reservoirs and receives natural flows, and the other pool (PT) is regulated and receives unnaturally high, cold water in summer; both pools are on the Trinity River, California. Thermal stratification formed in UT pool in spring at a critical flow of 1.01 m^3/s, peaked at 8.1°C in summer, and exhibited diurnal formation and destruction under sub-critical flows until fall. At PT pool, the 14.2 m^3/s baseflow caused mixing that prevented stratification and formed a spatially homogenous thermal environment. Statistical analyses indicated the daily range in air and inlet water temperature at UT pool best correlated with the occurrence and strength of stratification but were progressively irrelevant as flows increased above the critical value. The validated CFD model was used to reproduce the diurnal stratification and explain the processes involved. The CFD model correctly predicted the observed critical flow and replicated the dynamics of stratification at UT pool and isohyets observed at PT pool. The CFD results also confirmed that low flows are the main variable for stratification to form, and the daily range in inlet water temperature drives the strength of the thermal gradient. The model estimated a critical discharge at PT pool of 2.0 m^3/s, twice that for UT pool owing to its 2.6-times larger area, suggesting critical flows scale with pool size. Results showed that releasing critical and lower flows in summer on regulated streams may conserve water and provide thermal gradients that benefit poikilothermic species; alternately, higher than critical flows can prevent stratification where needed to improve water quality.

KEYWORDS

3D CFD modelling, Chinook salmon, flow regulation, statistical modelling, thermal stratification, water quality

1 | INTRODUCTION

Impacts to rivers by dams can be profound even when regulated flow releases are designed to mitigate downstream effects on a stream's biology (Swales, 1989). One type of mitigation involves flow releases in summer that are higher than pre-dam flows to provide colder water temperatures. This strategy is used on the Trinity River in northern California (Figure 1) to account for dams blocking spring Chinook salmon (*Oncorhynchus tshawytscha*) access to cold water for holding in pools in the upper watershed. The mitigation involves flow releases in July through September of 12.7 m^3/s that range in temperature from 9 to 11°C, which is more than double the median (5.4 m^3/s) flow and about 10°C colder than in the unregulated period of record for the Trinity River at Lewiston in summer (1911–1960). The high discharge provides spring Chinook cold water for holding (<15.6°C; USFWS & HVT, 1999) but has perhaps unforeseen negative consequences for the river biome, including salmonids (*Oncorhynchus* spp.).

An example serves this point. Consider the time for mayfly (*Ephemerella proserpina*) to hatch as adults inversely relates to temperature (Sweeney & Vannote, 1984). Since mayflies compose the largest percentage of diet for juvenile steelhead (*O. mykiss*) in the Trinity River (Boles, 1990), their suppression by cold water may negatively affect food availability for salmonids. Food assimilation and growth of juvenile salmonids generally increase with temperature to peaks around 17°C for coho (*O. kisutch*) and steelhead and 19–21°C for Chinook (Lusardi et al., 2019; Plumb & Moffitt, 2015). In comparison, the average daily water temperature in summer at the compliance point at Douglas City (Figure 1) in water years (WY) 2019–2021 was 13.1°C, suggesting food availability and juvenile growth may be suppressed by the cold water. Smaller juveniles often exhibit lower survival to adult (Woodson et al., 2013), so the objective for the high summer baseflows to benefit adult salmon may instead depress future populations.

Both warm and cold-water are necessary for species to thrive, and we hypothesise that summer baseflows that are closer to natural levels promote temperature diversity in part by enabling thermal stratification in deep pools. With stratification, water temperatures form a thermocline, with warmer water near the surface and in marginal

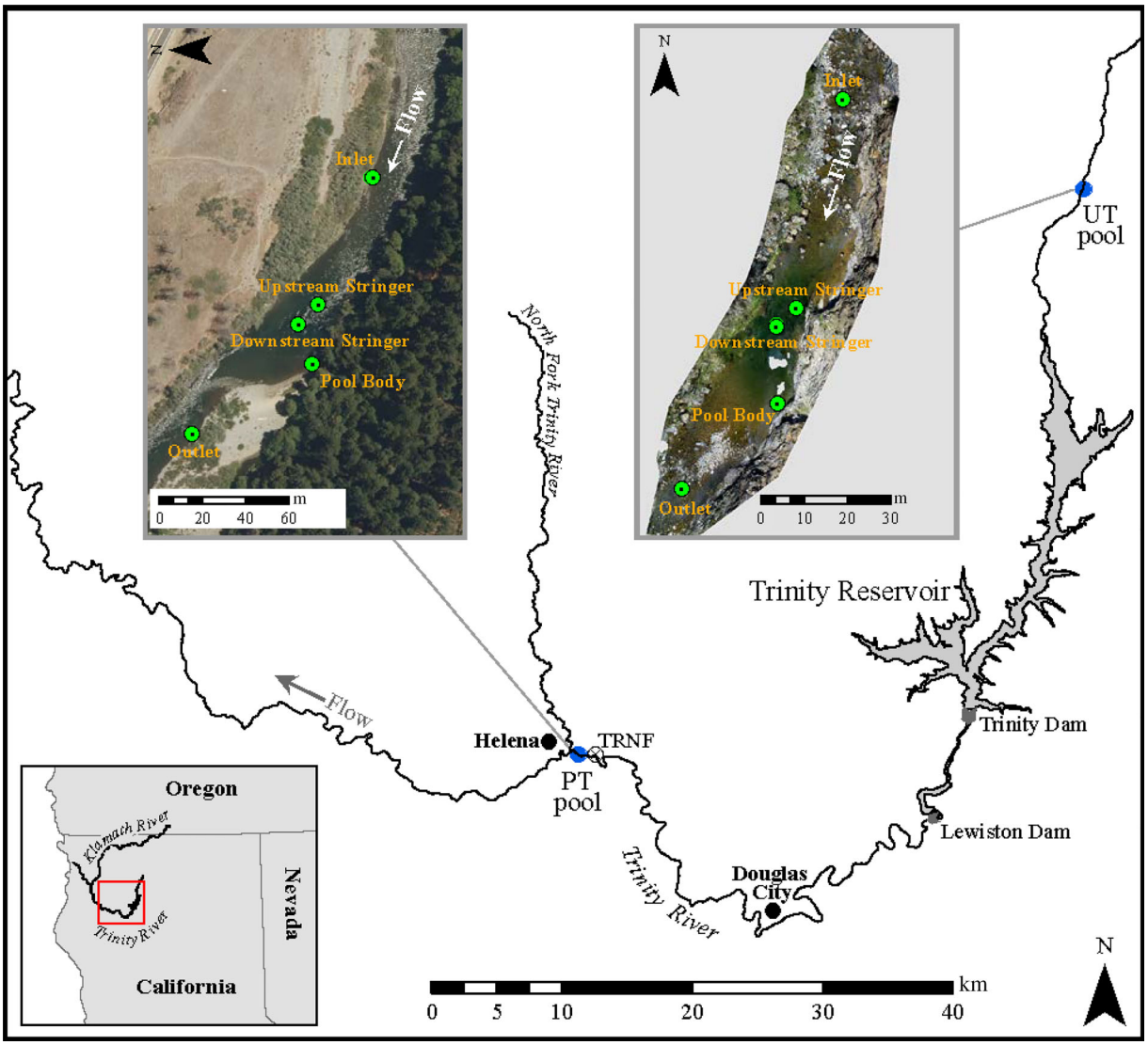

FIGURE 1 Location of study pools on the upper Trinity River (UT pool) and at the pear tree location on the Trinity River below Lewiston dam

areas for benthic invertebrates, juvenile salmonids, and other poikilotherms such as turtles and frogs, and cold water at depth for adult salmon and trout. However, thermal stratification can also occur with stratification of salt and dissolved oxygen that can make bottom water unsuitable for benthic macroinvertebrates and fish, as Turner and Erskine (2005) and Coates and Mondon (2009) observed in several regulated rivers in Australia. Therefore, while stratification may be important for species conservation in some settings, it may be desirable to prevent to improve water quality in others.

Temperature stratification is complex and may be controlled by many factors, but the mechanics of pool stratification have yet to be fully described in part because past work has been largely relational (e.g. Bilby, 1984; Keller et al., 1990). For example, Matthews et al. (1994) measured stratification in a deep pool on the American River, California and attributed it to retention of cold surface water delivered at night and other periods of low air temperature or reduced solar input. Nielsen et al. (1994) documented thermal stratification in pools on several California streams and associated its occurrence with input of cold hyporheic, spring or surface flows and low turbulence or obstructions preventing mixing in the pools. Butler (2013) associated stratification with low discharges in the San Jaoquin River, California and attributed its temporal variability to diurnal changes in air temperature and its spatial variability to topographic variations creating high and low velocity areas in the flow.

Several field studies with numerical modelling have further described conditions that influence thermal stratification in river pools. These include Borman and Webster's (1998) 2D modelling that reproduced laterally averaged temperatures at depth during stratification in a large pool (average 110 m wide, 5 m deep) on the River Murray, Australia; under a nearly constant flow (46.3 m^3/s), stratification persisted except when winds ≥10 m/s caused mixing that destratified the pool. Persistent stratification was also measured by Turner and Erskine (2005) in pools on several large rivers in Australia, where high winds (>8 m/s) and elevated flows (21.7–40.7 m^3/s) replaced the stratified water with mixed flow. Reinfelds and Williams (2012) associated stratification in pools on the Shoalhaven River, Australia with the Richardson number and found it was unaffected by wind and formed at around the median annual flow.

We add to this body of evidence for thermal stratification with a field study and statistical analyses of two pools on the Trinity River; findings are confirmed and supplemented by numerical modelling with the validated 3D CFD model U^2RANS. The study objectives are to (a) measure field conditions that form or prevent thermal stratification; (b) identify the relative importance of variables affecting stratification with statistical analyses; and (c) apply the 3D CFD model to predict the critical discharge for diurnal stratification and identify key variables that drive its formation, stability, and decay. Our CFD modelling is a first, to our knowledge, to study stratification in river pools in 3D and provides a means to estimate critical flows for stratification. With this ability, water managers can avoid both unnaturally low flows that enable stratification to degrade water quality and abnormally high flows that prevent stratification and produce a cold river that threatens salmon populations via the positive relationship between juvenile fish size and survival to adult. Given the societal and ecological importance of restoring salmon in North America and elsewhere, our particular interest is in whether scientific justification exists for lowering summer baseflows to natural levels on regulated streams to form temperature gradients in pools?

2 | METHODS

2.1 | Study sites

Field studies were undertaken in Summer 2020 to document flow and temperature conditions under which thermal stratification may exist or be prevented in two pools on the Trinity River. One pool (UT) is unregulated and located on the upper Trinity River above Trinity Reservoir (Figure 1). The other pool (PT) is located 63 km downstream of Lewiston Dam at Pear tree near Helena, California. Water is delivered to both pools primarily by surface flow with presumably small contributions from hyporheic sources. This presumption is based on the river being confined by mountains that inhibit lateral exchange of shallow groundwater; also, the channel exhibits a largely planar slope upstream of both pools that would limit hyporheic forcing to areas near boulders that only exist upstream of UT pool (e.g. Marzadri et al., 2012). The hyporheic flow in these places would likely have minimal effect on pool temperatures due to their short flow paths in shallow alluvium in the upstream vicinity of UT pool (see below). The channel slope at each pool's inlet (Figure 1) and the downstream hydraulic control is 0.40% at UT pool and 0.09% at PT pool. The field study occurred 10 June to 22 November 2020 at UT pool and 1 July to 5 November 2020 at PT pool.

2.2 | Pool surveys and descriptions

Detailed surveys were used to measure each pool's bathymetry for the 3D CFD modelling. The UT pool was surveyed with total station, Real Time Kinematic GPS (RTK), single beam sonar, and structure-from-motion photogrammetry in summer 2020. The SfM survey of dry land yielded over 179 million points with a vertical accuracy of ±0.03 m (95% confidence level [CL]; ASPRS, 2014). Over 45 million logically valid points were retained and subsampled in a 0.076 m grid that left 248,047 points in the final topography. Underwater SfM yielded 52,000 points with a vertical accuracy of ±0.08 m (95% CL). These were reduced to 30,610 points and combined with 3349 points from RTK and total station and 1979 points from sonar to yield an average density of 94 points/m^2. Surveyed elevations compared to known elevations at local controls indicated the survey's total vertical error was ±0.11 m (95% CL).

The PT pool and surrounding terrain was surveyed with multibeam sonar, lidar, and total station in 2016 by Pryor (2017). In Summer 2020, areas where changes in bathymetry may have occurred were resurveyed using single beam sonar and total station. These surveys combined with the 2016 surveys yielded an average density of 2.4 points/m^2 within the pool body where depths were ≥2 m and 1.7

points/m^2 for the entire resurveyed area. The final survey error was not measured across all data, but the total station error was ±0.01 m (95% CL), the sonar specifications are ±0.05 m (95% CL), and a surveyor statement on the 2016 topography specifies ±0.12 m (95% CL). All surveys were performed with the horizontal datum NAD83 and the vertical datum NAVD88 Geoid 09.

Channel elevations subtracted from the water surface elevation at summer baseflow indicated the pool area with depths ≥2 m is 505 m^2 at PT pool and 193 m^2 at UT pool (Figure 2). The ≥2 m depth criterion was from observations that temperature stratification occurs below around 2 m depth (e.g. Nielsen et al., 1994; Reinfelds & Williams, 2012). A cross section at the deepest location in each pool indicates summer baseflow at UT pool occurs in a narrower (12.2 m) and deeper (5.1 m maximum depth) channel compared to PT pool (31.2 and 4.4 m, respectively). The ratio of the width to surface area where depths are ≥2 m is 2.6 at both pools.

Topographic lines and a longitudinal profile through the centreline of each pool shows the UT pool entry transitions steeply to the pool bottom whereas the PT pool entry slopes gently into the pool body (Figure 2). Otherwise, similarities in the pool morphologies exist. For example, the left bank at UT pool is bedrock and the inlet area and pool bottom are shallow alluvium on a bedrock mantle that is exposed at the decline into the pool and in outcrops on both banks. The right bank of PT pool is also bedrock, and the inlet and pool body are alluvial. Both pool outlets are alluvial and gently slope to their downstream hydraulic control (Figure 2).

2.3 | Flow stage, discharge and temperature

Flow stages and temperatures were measured at each pool's inlet, body and outlet in 15 min intervals to ±0.4 cm and ± 0.44°C

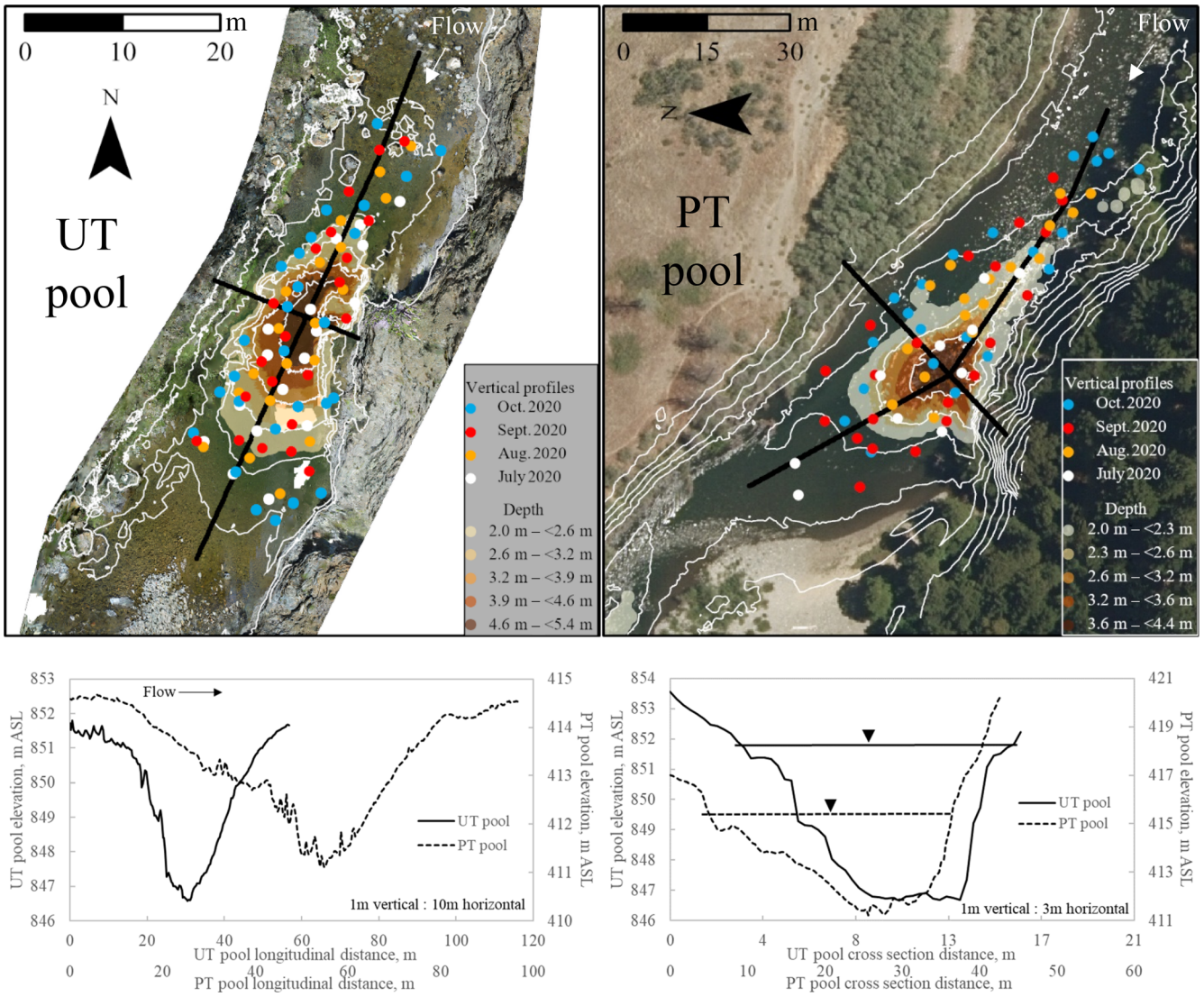

FIGURE 2 Planview of the UT and PT pools with topographic lines in one-metre increments and shaded areas where water depths at summer baseflow were ≥2 m. Longitudinal profiles and cross sections are labelled with their vertical exaggerations, and locations where flow velocity and temperature profiles were measured are shown. The summer baseflow water surface is plotted in the cross sections where the view is facing upstream. ASL is above sea level.

(manufacturer specifications) with a Hobo pressure transducer (Figure 1). The stages were assigned discharges by gaging the inlet of UT pool, which also provided hydraulic geometry relationships to flow at this location. The stage-discharge relationship at PT pool was developed with flows gaged by the U.S. Geological Survey (USGS) at a location 380 m upstream on the Trinity River above the North Fork Trinity River (TRNF; Figure 1). Reynolds numbers (Re; Equation 1) were computed with the measured hydraulic geometry at UT pool and the stage-discharge relationship and a cross section at PT pool to verify that flows at both pool inlets were turbulent and temperatures fully mixed using

$$\mathrm{Re} = \rho u D/\mu \quad (1)$$

where ρ is the water density, u and D are the average cross section velocity and depth, respectively, and μ is the dynamic viscosity of water. Additionally, air temperature was measured adjacent to each pool at a height of 1.5 m from the ground in the shade of trees. Two cameras were installed at the UT pool to monitor the above equipment and document its surface exposure to sun every 30 min from sunrise to sunset. One camera with a full upstream view of the PT pool was installed for these same purposes.

The ratio of flows gaged at UT pool ($n = 7$) to flows measured at the same time of day by USGS at a location 7 km downstream on the Trinity River (0.53; range 0.46–0.58) was used to adjust the record of daily average flows in July–October for WY 1958–2021 at this station. The adjusted flows were used to estimate the exceedance probability of the observed critical flow for stratification at UT pool in these months. Stratification was not observed at PT pool and an exceedance probability was not determined for the modelled critical flow because discharges in the period of record (WY 2005–2021) at TRNF were substantially higher.

2.4 | Flow velocity and temperature profiles

Flow velocity profiles were measured in 3D at each pool with a Nortek acoustic Doppler velocimeter (ADV) to ±1 mm/s. The ADV was mounted on a 6 m adjustable rod for placement at surveyed locations at the desired height above the bed and for measuring the total depth to ±0.8 cm. Velocities were then recorded in easting, northing, and vertical coordinates at 8 Hz for ~5 min with a nominal velocity range of 0.01, 0.1, or 0.3 m/s, depending on flow speed. Temperature profiles were simultaneously measured with a Hobo temperature logger (±0.21°C) mounted on the downstream side of the rod to prevent interference in velocity readings. Depending on the total flow depth, 2−7 temperatures and time-averaged velocities were measured in a profile, and profiles were measured in monthly events from July through October 2020 at both pools. An exception is that temperature profiles were not measured in PT pool in July because the temperature logger was not available for mounting on the rod.

An ADV measures velocities with impressive accuracy, but false spikes in velocity can occur. We omitted these errors with a two-stage filter in software developed by Jesson et al. (2013). The initial filter omitted velocities when the correlation between paired echoes emitted from the ADV and reflected to the instrument by particles in the flow was <90% and the signal to noise ratio was >30 db. The second filter excluded values that were more than five times the standard deviation of the mean velocity, which was considered appropriate given the low average velocities (~0.04 m/s) at UT pool. A 12-point polynomial interpolation was used for spike replacement. Typically, more than 97% of the roughly 2400 instantaneous velocities in each gaging passed both filters and were used to compute a time-averaged velocity in easting, northing, and vertical directions. The square root of the sum of each averaged velocity squared gave the velocity magnitude. A total of 350 and 260 average velocities were measured in 81 and 70 vertical profiles at UT and PT pool, respectively (Figure 2).

A time series of water temperatures was measured in vertical profiles with stringers of temperature loggers in UT and PT pool. A "downstream" and "upstream" stringer was installed in each pool, and both stringers included a cable that extended from a weight at the pool bottom to a float at the surface that held the cable nearly vertical in the flow. The upstream stringer at UT pool had a Hobo temperature logger attached to the cable at depths of 0.9, 1.9, 2.8, 3.4 and 4.0 m and on the channel bed at 4.6 m depth at summer baseflow, and the downstream stringer had loggers attached at depths of 0.9, 1.9, 2.8, 3.4 and 4.0 m and on the channel bed in 5.1 m depth. An "upstream" and "downstream" stringer of loggers was also deployed at PT pool where the depth at summer baseflow was respectively 4.1 and 4.0 m; these stringers had loggers attached to the bottom weight and the cable at depths of 0.4, 1.4, 2.3, 2.9 and 3.5 m. The loggers recorded a temperature every 15 min for the study period at UT pool and 1 July–6 August 2020 at PT pool. The measurement duration at PT pool was relatively short due to theft of the equipment.

The degree of stratification (S_d) is the range of water temperatures in a vertical profile (Reinfelds & Williams, 2012). We considered stratification as formed when $S_d \geq 1.0$°C, which corresponds to a temperature gradient of ≥ 0.20°C/m at UT pool and ≥0.24°C/m in PT pool. These values agree with definitions of stratification that Reinfelds and Williams (2012; 0.20°C/m) and Sherman et al. (1998; 0.25°C/m) used. In profiles with stratification, a thermocline occurs at the base of the epilimnion; this level defines the thermocline depth. The thermocline thickness extends from the depth of stratification through the metalimnion and hypolimnion to the pool bottom. Surface areas in UT pool with stratification were measured in ArcPro with the terrain maps by interpolating between verticals that either displayed or lacked a thermocline using the bathymetry and water depths as guides (Figure 2).

2.5 | Statistical analyses

A standard procedure for statistical model selection was used to assess the evidence of factors associated with the occurrence and strength of stratification in UT pool. PT pool was not included in the statistical modelling because stratification was not observed there. For UT pool, the continuous response variable was the daily maximum S_d (S_{dmax}). Potential explanatory variables included the (a) daily air

temperature differential (DATD) computed as the difference in each day's maximum and minimum air temperature; (b) mean daily inlet water temperature (MDIWT); (c) daily inlet water temperature differential (DIWT, computed as for DATD); (d) daily average flow (Q_{avg}); (e) day length (DL) as duration between sunrise and sunset at UT pool; and (f) sun exposure (SE) as duration when the pool surface was in direct sunlight. Given the likelihood that temporal autocorrelation would violate the assumption of independence of errors in the regression, residual analysis using the autocorrelation function (ACF) and partial autocorrelation function (PACF) plots was applied to evaluate the need for a time-series variance component to our model, and if so, whether auto-regressive, moving average, or both forms should be incorporated (Chatfield, 2003).

For each candidate model, an akaike information criterion (AIC) value was calculated. The AIC is a statistic that combines a measure of model fit quality that lowers the AIC value or applies a penalty for model complexity that increases the value. Additional parameters that do not improve quality of fit simply inflate the AIC value, and so lower AIC scores indicate preferred models. The simplest model within two AIC units of the best scoring model was selected for inference at each step using the following procedure. The variance component structure was held constant during the model selection process, although the variance parameters would be estimated along with each model's fixed effects parameters. During the model selection process, combinations of explanatory variables prone to multicollinearity were avoided. First, models containing each of DATD, MDIWT, and DIWT were compared to evaluate evidence for which variable(s) best explained S_{dmax}. In the second step, Q_{avg} and each of DL and SE were added to the model arising from the first step to evaluate evidence for increased quality of model fit. In the third step, if the model arising from step-two contained more than one explanatory variable, then AIC would be further used to evaluate whether interaction terms were warranted. Finally, once a model was selected, acf and pacf plots were used to assess the final variance component structure, and AIC was used to finalise evidence of any changes suggested by those plots. All statistical analyses were carried out using R Statistical Software (R Core Team, 2021), and parameter estimation was conducted via generalised least squares using the *nlme* package (Pinheiro et al., 2021).

2.6 | Numerical modelling

The CFD model U^{2}RANS, developed and validated by Lai et al. (2003) and further validated by Lai et al. (2021) and Lai (2022), was applied to simulate the dynamics of thermal stratification at the study sites. The CFD model has also been validated at the pools in this study; the theory and validation results for the model were reported by Lai et al. (2022); therefore, only a summary is provided here. The numerical modelling was used to (1) quantify the relationship between pool stratification and river flow so that the critical discharge at stratification may be determined and (2) to identify the dominant processes that control stratification at the study sites. The model solves the Unsteady Reynolds-Averaged Navier–Stokes (URANS) equations based on the mass, momentum, and energy conservation laws. The Navier–Stokes flow equations are standard and described in Lai et al. (2022). The energy conservation equation for water temperature is

$$\frac{\partial T}{\partial t}+\frac{\partial (U_j T)}{\partial x_j}=\frac{\partial}{\partial x_j}\left(\alpha\frac{\partial T}{\partial x_j}-\overline{T'u_j}\right)+\frac{q_s}{\rho C_P} \quad (2)$$

where t is time, x_j is the jth component of the Cartesian coordinate, T and T' are the mean and fluctuating water temperature, U_j and u_j are the jth components of the mean and fluctuating velocities, α is fluid thermal diffusivity of water, q_s is the heat exchange rate at the stream surface owing to meteorological forcing such as solar radiation, and C_p is the specific heat capacity of water. The numerical solution utilised an unstructured 3D mesh on which the governing equations were discretized and solved. The total number of mesh cells was 150,698 for UT pool and 212,038 for PT pool and the vertical mesh size was 0.076 m at both pools. Coarser and finer meshes were also modelled, with results indicating mesh convergence.

Two important issues are discussed as they were not reported in Lai et al. (2022). First, the thermal diffusion due to turbulence (or turbulent heat flux) in Equation (2) was computed as

$$-\overline{T'u_j}=\frac{\upsilon_t}{P_{rt}}\frac{\partial T}{\partial x_j} \quad (3)$$

where υ_t is the turbulence viscosity and P_{rt} is the turbulent Prandtl number. The turbulence viscosity is computed using the standard $k-\varepsilon$ turbulence model (see Lai et al., 2022). The Prandtl number is a model parameter whose value is usually determined by comparison with field data. In this study, we adopted the final value of P_{rt} determined by Lai et al. (2022) and listed in Table 1. The second issue regards the role of heat exchange rate at the stream surface (q_s in Equation 2). In general, surface heat exchange from meteorological forcing is the dominant process that controls how water temperature varies temporally in a stream. Such forcing was incorporated by applying the measured water temperatures at the pool inlet boundary. The extra surface heat exchange within the pool was found negligible for stratification in separate numerical modelling performed with and without the forcing term (see Supplementary Information). This results because the convective and diffusive heat transfer processes dominate the pool stratification at the study sites. Put another way, the surface area of the river upstream of the pool is very large relative to the pool surface area, so meteorological forcing (and discharge) that controls water temperatures and the stratification process is captured at the inlet boundary condition. Additional model inputs included topography of the pools and stage (water elevation) at the pool outlets.

3 | RESULTS

3.1 | Upper Trinity River pool

Vertical temperature profiles measured with the upstream and downstream stringer at UT pool gave similar results, and data from the

TABLE 1 CFD model parameters for critical flow estimates and sensitivity analysis

Time step	Turbulent Prandtl number	Turbulence model	Vertical mesh size	Water density	Specific heat capacity
1.0 s	45.0	k–ε model	0.076 m	1000 kg/m^3	4180 J/(kg K)
Location	Application	Dates	Discharge (m^3/s)	Average inlet water temperature (°C)	Inlet water temperature range (°C)
UT pool	Estimate critical flow	18–19 July 2020	1.03 and 1.55	21.6	17.8–26.5 (8.7°C)
	Sensitivity analysis	NA	0.52		17.8–25.5 (8.7°C)
					19.2–24.6 (5.4°C)
					20.6–22.8 (2.2°C)
PT pool	Estimate critical flow	29–30 July 2020	1.42, 2.0, 2.5	19.9	17.2–22.3 (5.1°C)

downstream stringer are in Figure 3. Results for the upstream stringer are in Figure S1. Stratification formed in UT pool at S_d ≥1.0°C for the first time on 28 June at 12:30 PM when the daily average flow was 1.01 m^3/s (Figures 3 and S2). The exceedance probability of this critical flow represented as a daily average value was 33% in July–October in WY 1958–2021. In addition, the average and longest period of the day with S_d ≥1.0°C was respectively 8.3 and 13.0 h. This information suggests that thermal stratification is a common occurrence in summer and early fall at UT pool. After 28 June, stratification formed daily between 11:15 AM and 2:15 PM and was destroyed between 1:30 PM and 11:45 PM (Figure 3). Differences in the timing and duration of stratification resulted from hot weather causing stratification to form earlier and last longer in the day compared to cooler weather that caused the opposite. Values of Re were ≥ 17,480 in the study period, indicating inlet flows were fully turbulent and temperatures well mixed when entering the pool.

After stratification first established, a daily cycle of formation and destruction ensued. The cycle is described with temperatures at the downstream stringer on 31 July (Figure 4), which represent thermal dynamics observed for most of the study period (e.g. Figure S3). At midnight, water temperatures at the pool inlet and outlet and all depths in the pool were ~ 20.2°C and approximately equal (±0.10°C). Temperatures decreased through sunrise at 6:00 AM until ~9:00 AM when the daily minimum occurred (16.6 ± 0.10°C). Between midnight and 9:00 AM, the pool stored cold inlet water and released warmer water downstream perhaps from storage in lee areas of the pool. At 9:45 AM, S_d departed the nighttime range of 0.18 ± 0.01°C when cameras documented the river's first exposure to direct sunlight. At this time, the pool began releasing relatively cold water downstream and a thermocline formed in UT pool and expanded vertically until ~4:30 PM when the pool surface temperature (25.0°C) and S_d (7.3°C) peaked. Shade from mountains and trees then began to cover the river bottom (orange area, Figure 4) and when the river was half shaded, inlet temperatures dropped below temperatures in the epilimnion and began to mix with deeper layers in the pool. This displaced the warmer top water and returned the pool to storing cold water and releasing warmer water downstream. The mixing continued to destabilise the stratification until just before sunset at 9:00 PM when the thermal layering was destroyed and temperatures at all depths differed by only 0.07°C (grey area, Figure 4).

Thermoclines indicating thermal stratification predominantly formed in deeper water but were in increasingly shallow areas of UT pool as discharge lowered through summer (Table 2, Figure 5). Discharge lowered even further in October, yet thermocline depths increased and were no longer related to water depth likely due to water temperatures decreasing into fall. For example, a thermocline did not develop in October where the depth was 5.1 m in the middle of the pool but was measured near the right bank in the lee of a bedrock outcrop where the depth was 3.3 m. This supports Nielsen et al. (1994) and Butler's (2013) observation that pool bathymetry that creates low velocity areas can affect where stratification forms, particularly outside the heat of summer as we measured.

When stratification was present, flow velocities in the epilimnion of UT pool were ~ 10 cm/s and velocities in the stratified body of the pool were <2 cm/s, indicating a cold, slow water body existed below a warmer, faster top flow. Thermocline depths and thicknesses were also largely consistent in the study period even though pool areas with stratification increased through summer and reduced in fall (Table 2). The average thermocline depth (2.0 m) that we measured agrees with what Nielsen et al. (1994) observed in pools that were around 4 m deep on the Middle Fork Eel River, California and close to what Reinfelds and Williams (2012) measured (2.2 m) in a 15 m deep pool on the Shoalhaven River, Australia. Similar thermocline depths across studies result from the exponential decay in penetration of solar radiation in water.

The ending of the stratification period occurred between 9 and 11 November. In this period, night air temperatures dropped below freezing (−1.2 to −2.7°C) and daytime air temperatures rose to 11.1°C, which raised inlet water temperatures to 11.3°C (range 4.3–5.6°C). This enabled stratification to reform daily, but for the last time when daily average flow was 0.31 m^3/s and S_d = 1.8°C on 11 November (Figure S4). Later, on 20 and 21 November, inlet water temperatures ranged 3.0–3.3°C but stratification failed to reform perhaps because the difference in buoyancy between temperatures (≤0.10 N/m^3) was too small to stratify at the observed flows (0.69 and 0.52 m^3/s).

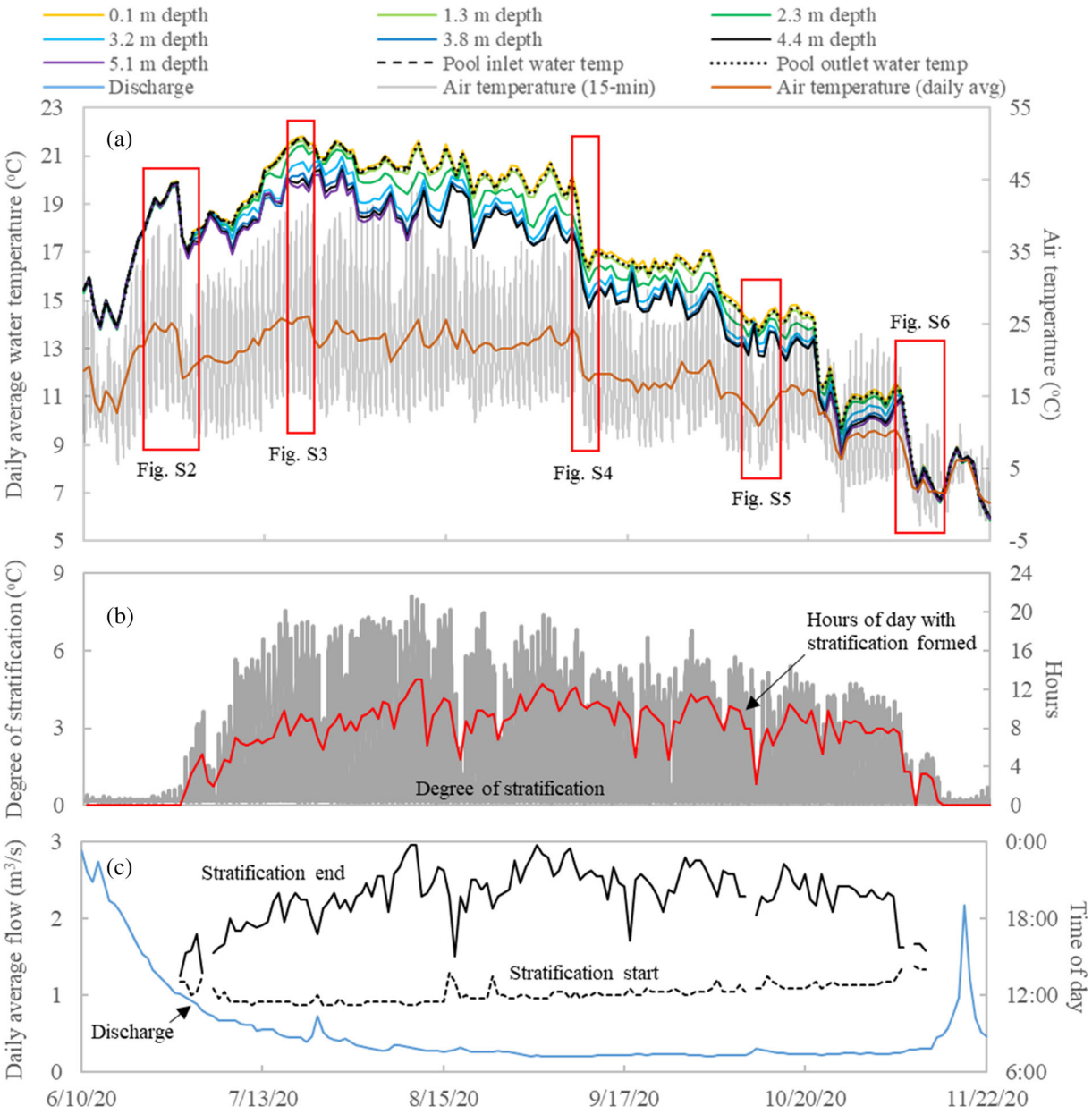

FIGURE 3 Daily average water temperatures measured at the UT pool inlet and outlet and vertically in the pool with the downstream stringer (a) air temperatures measured every 15 min and averaged by day are also shown. (b) The degree of stratification measured vertically in the pool every 15 min and the proportion of day the temperature range exceeded 1.0°C, indicating formation of thermal stratification. (c) The time of day that stratification started and ended daily and the daily average flow through the pool.

3.2 | Pear tree pool

Vertical temperature profiles measured with the up- and downstream stringer were nearly identical and results for the upstream stringer are presented in Figure 6. As at UT pool, diurnal variations in water and air temperature occurred at PT pool when the stringers were installed (1 July–5 August, Figure S5). Within these dates, the mean daily average flow was 14.63 m^3/s (range 13.90–16.71 m^3/s) and the highest daily average air (24.7°C) and inlet water temperatures (20.7°C) of the study period were recorded; the range in air (8.2–20.1°C) and inlet water temperatures (2.5–5.1°C) were also respectively close to or exceeded ranges observed in the remainder of the monitoring period (6 August–5 November; 7.0–22.0°C; 1.0–4.9°C). Stratification was therefore most likely to form when the upstream stringer recorded temperatures, yet S_d ranged only 0.05–0.36°C and pool inlet and outlet temperatures matched temperatures in the stringers, indicating complete thermal mixing in the pool by the high summer baseflow (Figure S5). Temperatures were also fully mixed at the pool inlet where values of *Re* were ≥ 229,662 during the study.

In close agreement with stringer temperatures, S_d ranged 0–0.48°C in vertical profiles measured with the Hobo logger mounted on the flow rod (Figures 2 and 7). Temperatures in the isotherms did

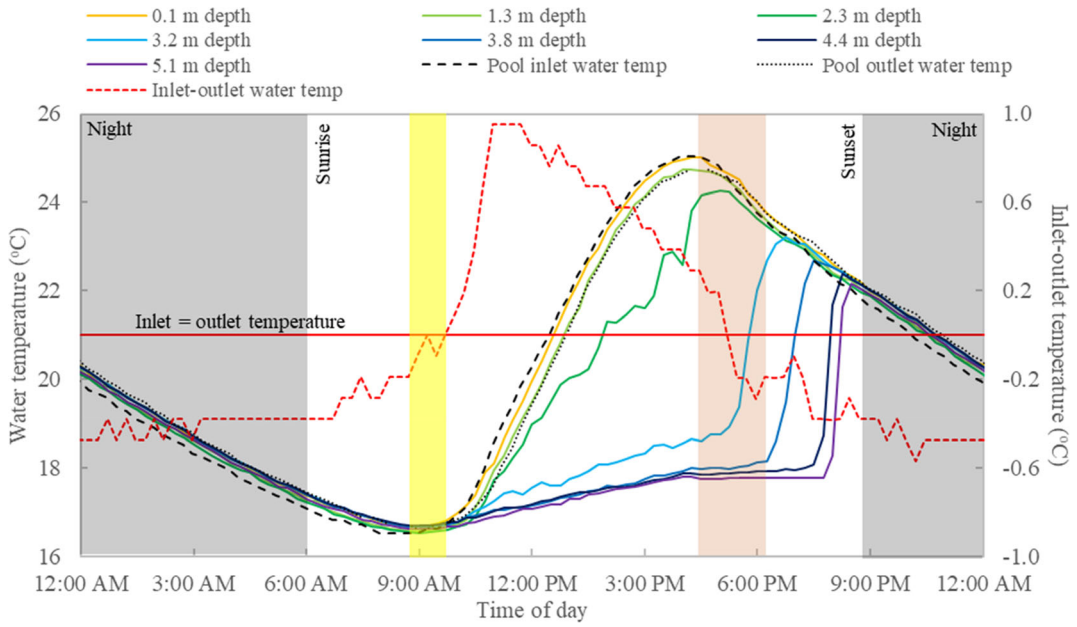

FIGURE 4 Formation and destruction of thermal stratification at the UT pool on 31 July 2020. The figure shows night times shaded black, periods when direct sunlight first contacted and then fully covered the river bottom shaded yellow, and the time for shade from mountains and trees to first contact and then fully cover the river bottom shaded orange. Sunrise and sunset times at UT pool were provided by suncalc.org.

TABLE 2 UT pool depths where thermoclines were not observed or present with their attributes and estimated area of stratification in the pool

Dates	Flow (m^3/s)	Depths with thermocline (m)	Depths without thermocline (m)	Thermocline depth (m)[a]	Thermocline thickness (m)[a]	Pool area with stratification (m^2)
July 30–31, 2020	0.37	≥4.0	≤2.8	1.5–2.9 (2.2)	1.8–2.7 (2.2)	88
Aug. 25–26, 2020	0.30	≥2.5	≤2.5	1.6–2.2 (1.8)	0.9–3.4 (2.0)	116
Sept. 22–24, 2020	0.31	≥2.3	≤2.3	1.2–2.1 (1.8)	0.9–3.2 (1.9)	133
Oct. 13–15, 2020	0.32	≥3.3	≤5.0	2.0–2.2 (2.1)	1.2–2.8 (1.9)	65

[a]Range of observed values with average in parenthesis.

vary because of diurnal variations in pool temperatures and profiles being measured at different times of day (Figure 7, S5). Flow velocities in the vertical profiles generally increased with distance from the bed and were mostly around 1 m/s.

Two notable changes in river flow affected diurnal temperatures in PT pool during the study period. The first change in flow occurred 13–20 September when Lewiston Dam releases were raised from the 12.70 m^3/s baseflow to 29.45 m^3/s to assist Chinook salmon in the lower river (Figure S6). The higher flow muted diurnal changes in water temperature and lowered the daily peak temperature by 3.4°C compared to the day after baseflow resumed. Another flow change occurred discharge was lowered to winter baseflow (8.49 m^3/s) on 14–17 October; the decrease had no noticeable effect on the temperature variations or the daily peak temperature (Figure S7).

3.3 | Statistical modelling

The first step in selecting a statistical model for explaining the observed variation in S_{dmax} involved assessing the potential for multicollinearity, which is done to avoid fitting models with excessive correlation amongst explanatory variables. This yielded a set of candidate models with up to three explanatory variables (Table 3). The model fitting revealed strong evidence for temporally autocorrelated residuals and showed an autoregressive order-1 (AR[1]) time series variance component was appropriate due to the trailing decay pattern of the ACF plot and abrupt cut-off after lag-1 in the PACF plot (Chatfield, 2003; Figure S8, S9). Of the first main effects models, there was strong support by the AIC to proceed with the model containing DATD (Table 3, Step 1, ΔAIC^1), and again support that both Q_{avg} (Table 3, Step 2, ΔAIC^1) and the interaction of Q_{avg} and DATD improved the quality of fit enough to retain these variables (Table 3, Step 3, ΔAIC^2). Finally, the acf and pacf plots for the selected model revealed that an AR(1) structure remained the proper variance component structure (Figure S10, S11).

The estimated model parameters provide evidence of the importance of an interaction between Q_{avg} and DATD (Table 4, p-value = 0.026), which complicates interpretation of each variable on its own. The effects of interacting variables are best explained via an interaction plot, which suggested that DATD has a strong effect on

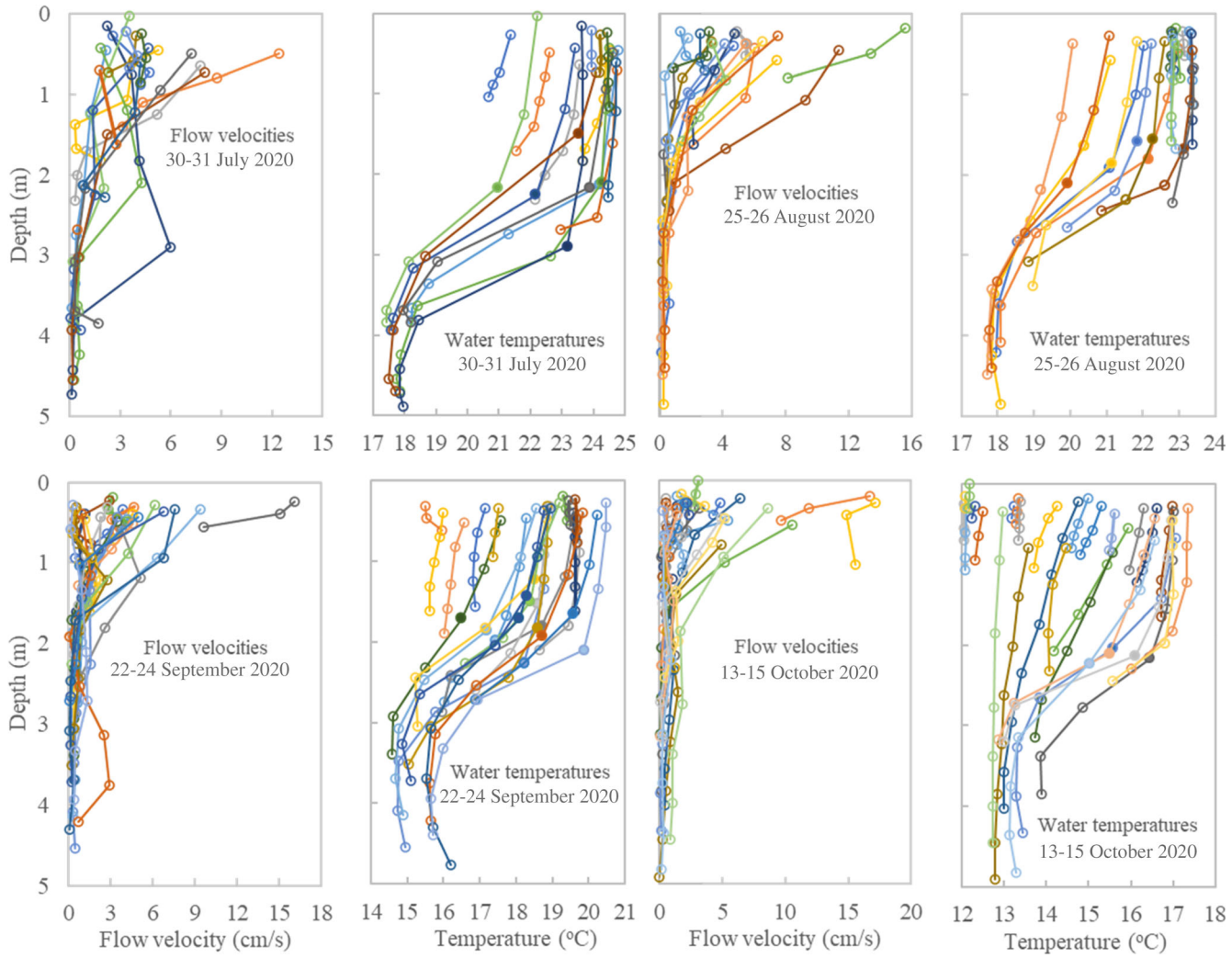

FIGURE 5 Vertical velocity and temperature profiles at UT pool in July through October 2020 (also see Table 1). The thermocline depth in the temperature profiles is marked with filled symbols.

S_{dmax} at relatively low discharges (Figure 8). However, as discharge increases to even moderate levels, the estimated effect of DATD decreases to the point of displaying little to no estimated effect. Results also suggest that S_{dmax} will always be relatively low at higher discharges, regardless of DATD, and that relatively high values of S_{dmax} can only be achieved when DATD is high and discharge is low. The same applies to a competing model with DIWT (Figure 8, Table 4).

3.4 | Numerical modelling

The 3D CFD model was shown by Lai et al. (2022) to predict temperatures at the UT and PT pool that closely agreed with the field results, validating that the CFD model is adequate for the present study. For example, temperature results at 0.52 m^3/s in UT pool during 18–19 July, 2020 were within 0.5°C of temperatures measured at all depths in the downstream stringer over 85% of the time (Figures 9 and S3). The remaining 15% of the time, temperature differences were up to 1.8°C primarily at the beginning period of pool stratification formation. At PT pool, the model predicted isotherms that were observed in the field, and temperature differences between the simulated and measured profiles were ≤0.25°C at 14.24 m^3/s on 29–30 July, 2020.

The validated CFD model was used to estimate a critical discharge for stratification at UT and PT pool. At UT pool, the daily range in temperature was held the same as observed on 18 and 19 July and two additional discharges were simulated (1.03 and 1.55 m^3/s; Figure 10). The results indicate that the critical flow when $S_d \geq 1.0$°C was ~1.03 m^3/s, which is functionally equivalent to the observed discharge (1.01 m^3/s) that first enabled stratification on 28 June. This further coincides with field measurements indicating stratification being prevented at discharges above 1.0 m^3/s before this date (Figure S2). Modelling was also used to estimate a critical flow for stratification at PT pool by again holding inlet temperatures the same as observed on the above dates constant and varying discharges from 1.42, 2.0, and 2.5 m^3/s (Figure 11). The results indicate that

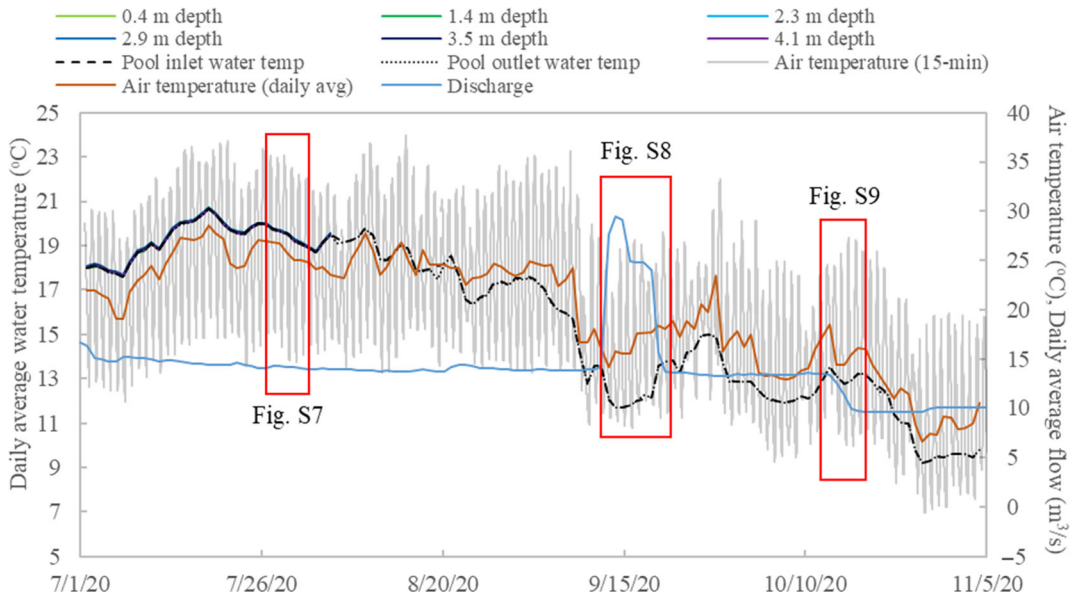

FIGURE 6 Discharge and air and water temperatures at PT pool. The water temperatures were measured from 2 July to 6 August with the upstream stringer where the pool depth was 4.1 m at summer baseflow.

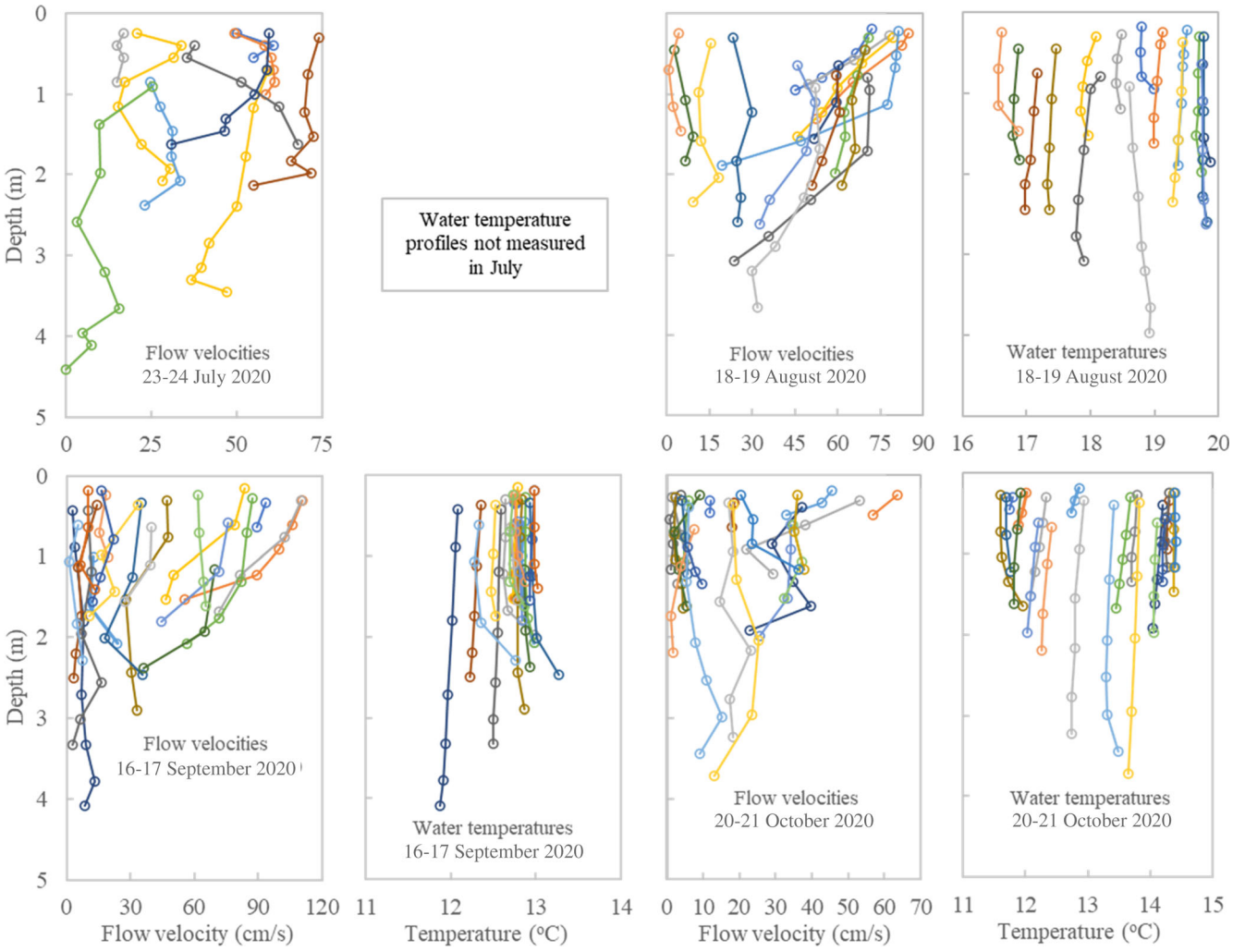

FIGURE 7 Vertical velocity and temperature profiles at PT pool

stratification forms at around 2.0 m^3/s, which is two times the critical flow at UT pool. The higher critical discharge at PT pool results from its greater size reducing thermal mixing by inlet velocities at a given flow.

The CFD model replicated the observed diurnal formation and destruction of stratification (Figures 9–11). This emphasises that while day and nighttime variations in solar radiation and air temperature produce diurnal changes in inlet water temperature, such meteorological forcing only implicitly drives the process of thermal stratification in river pools. Instead, we find that after discharge, diurnal variation in inlet water temperatures is the most significant factor in controlling whether stratification forms and the degree to which it strengthens in daytime. To demonstrate this, UT pool was modelled with discharge and mean inlet water temperature held constant at 0.52 m^3/s and 21.6°C and the amplitude of the diurnal change in temperatures varied from 8.7, 5.4, and 2.2°C (Figure S12). The S_{dmax} in these respective runs was 7.0, 4.5, and 1.6°C, confirming that stratification is stronger and temperature diversity greater in pools that are subjected to wider variations in inlet water temperatures at sub-critical flows.

Modelled and observed water temperatures at the inlet, outlet, and epilimnion of UT pool were close to the same values when stratification was formed, suggesting convective processes dominate as inlet water transits the upper layers of the pool (Figures 4 and 9). Under these conditions, a slow mixing period starts shortly after incipient stratification at ~9:00 AM when the pool bottom temperature begins to increase much more slowly than the pool surface temperature. The exchange of heat during this period is due primarily to the vertical diffusion process, which explains the slowness of the thermal mixing rate. Temperature stratification during the slow-mixing period is very stable and typically maintained for 6 h or longer. At about 4:00 PM, the inlet water temperature and so also the pool surface temperature reaches its daily maximum and begins to decline. Later, around 5:30 PM, the pool enters a rapid-mixing period characterised by a swift increase in pool bottom temperature over 3 to 3.5 h. This dynamic results primarily from unstable stratification when the surface water temperature drops below the temperature of water beneath it. Mixing by the unstable stratification is controlled by vertical convection collapsing the temperature gradient, as Butler (2013) observed. The breakdown is completed when temperatures at the pool bottom and surface converge, indicating the end of the stratification and return to the well-mixed state.

TABLE 3 Model selection results and AIC values for evaluating evidence of variables associated with pool stratification

Explanatory variables	*k*	AIC	ΔAIC^1	ΔAIC^2
Step 1: AR(1) variance component				
DIWT	4	161.09	3.27	25.81
DATD	4	157.82	0	22.54
MDIWT	4	161.26	3.44	25.98
Step 2: AR(1) variance component				
DATD, Q_{avg}	5	138.56	0	3.28
DATD, SE	5	159.75	21.19	24.47
DATD, DL	5	154.69	16.13	19.41
DATD, SE, Q_{avg}	6	139.65	1.09	4.37
DATD, DL, Q_{avg}	6	139.71	1.15	4.43
Step 3: AR(1) variance component				
DATD, Q_{avg}, DATD:Q_{avg}	6	135.28		0

Note: The AIC is a statistic that balances quality of model fit with complexity, and smaller AIC values indicate preferred models. Explanatory variables include daily air temperature differential (DATD), mean daily inlet water temperature difference (MDIWT), daily inlet water temperature differential (DIWT), mean-daily discharge (Q_{avg}, $\log_e$ transformed), day length (DL) and sun exposure (SE). A colon (:) indicates an interaction term amongst variables. *k* is the number of estimated parameters for each model. ΔAIC^1 compares the various AIC values to the lowest value for each step, and ΔAIC^2 compares the various AIC values to the lowest value amongst all models.

4 | DISCUSSION

Our hypothesis that natural summer baseflows can promote temperature diversity by enabling thermal stratification in river pools was proven by field measurements and CFD modelling at UT pool where baseflows are unaffected by flow regulation. In contrast, the high, regulated summer baseflow at PT pool created a spatially homogenous thermal environment where temperatures varied only from diurnal changes in solar input. The spatially uniform temperatures prevent juvenile salmonids from preferentially occupying different water temperatures in daytime when stratification would otherwise be formed in PT pool and presumably other pools between PT pool and Lewiston Dam. This may limit fish growth given that it is most energetically

TABLE 4 Parameter estimates for models with DATD or DIWT and Q_{avg} ($\log_e$ transformed) with their respective interaction

Model with DATD				Model with DIWT			
Variable	Estimate	Standard error	*p*-Value	Variable	Estimate	Standard error	*p*-Value
Intercept	2.53	0.61	<0.001	Intercept	1.71	0.78	0.03
Q_{avg}	−2.27	0.73	0	Q_{avg}	−1.63	1.05	0.13
DATD	0.02	0.02	0.54	DIWT	0.15	0.09	0.09
Q_{avg}:DATD	−0.07	0.03	0.03	Q_{avg}:DIWT	−0.27	0.12	0.03

Note: The estimated autoregressive order-1 parameter was 0.74.

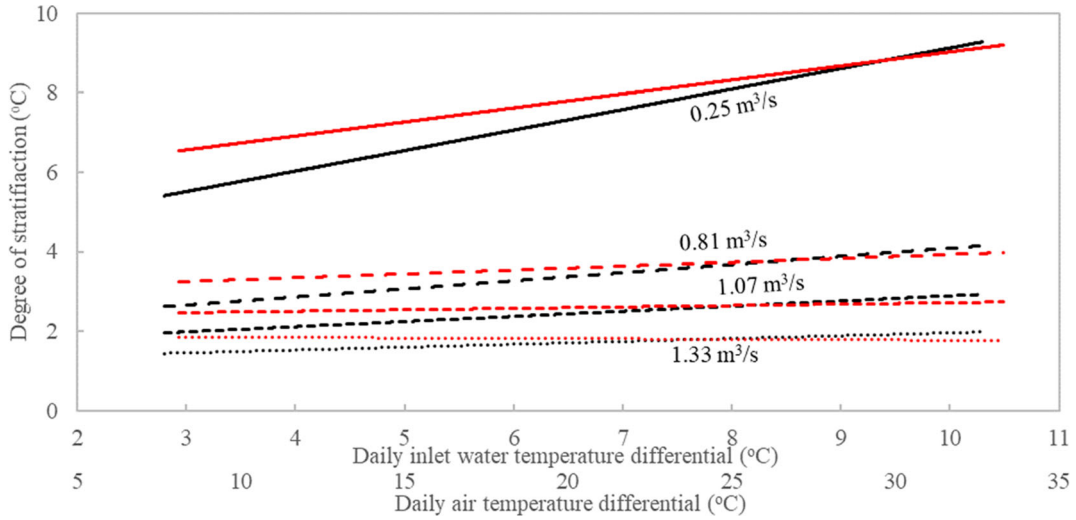

FIGURE 8 Interaction plot showing how discharge alters the estimated effect of daily air temperature differential (DATD, red lines) and daily inlet water temperature differential (DIWT) on the degree of pool stratification

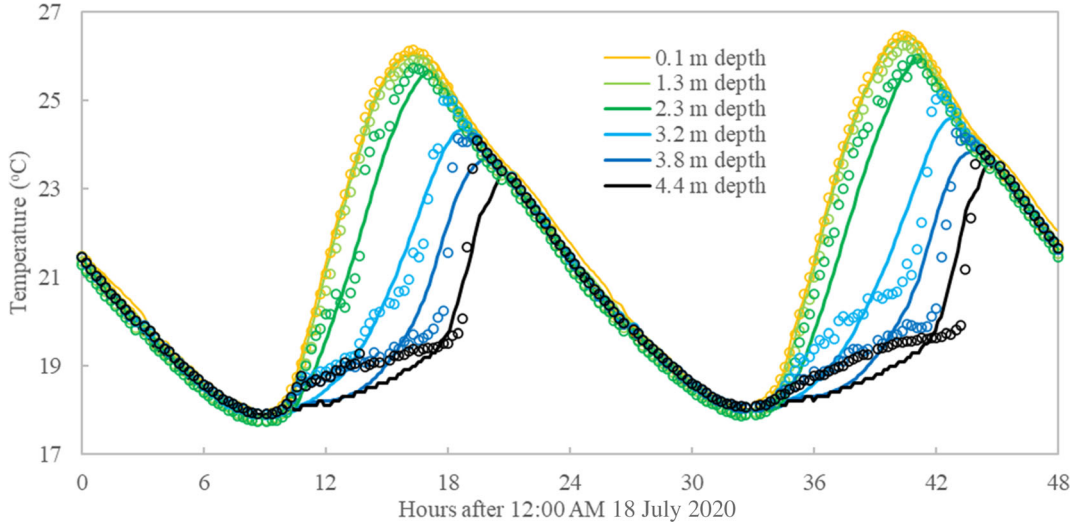

FIGURE 9 Observed temperatures in the downstream stringer on 18–19 July (open symbols) and temperatures predicted with U^{2}RANS (lines) on these dates. Figure reproduced from Lai et al. (2022).

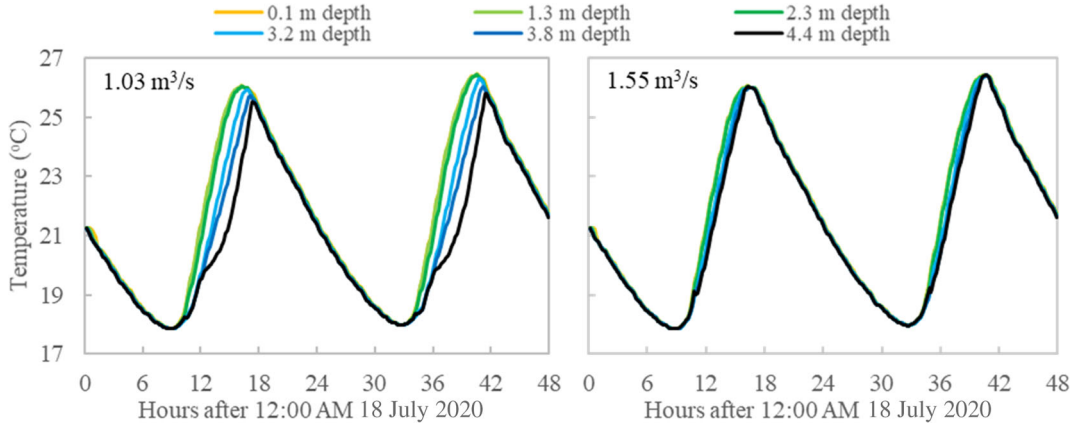

FIGURE 10 Predicted temperatures at the downstream stringer in UT pool

profitable for juvenile salmonids to forage in daytime bouts and then rest in relatively slow, warm water to maximise growth (Metcalfe et al., 1999). Alternately, when food is lacking, juvenile salmonids seek colder water to lower their metabolic rate and conserve energy (Sauter et al., 2001). Such temperature diversity is not available to fish in PT pool because the high summer baseflow mixes temperatures in the pool.

At PT pool, the CFD modelling predicts the diurnal variation of ~5°C in inlet water temperature would enable stratification and maintain cold water at depth for a larger proportion of the day at 1.42 m^3/s than we measured at ~14.2 m^3/s (Figure 11, S5). The lower baseflow would also enable water at the pool surface and margins to warm and benefit species that rely on external sources for body heat. This includes the Western Pond turtle (*Actinemys marmorata*) whose growth rates in summer on the regulated portion of the Trinity River are a fraction of those in the unregulated and much warmer South Fork Trinity River (Snover et al., 2015). Studies have also shown the unnaturally high baseflow delays Foothill yellow-legged frog (*Rani boylii*) development so that froglets often have too little time for growth

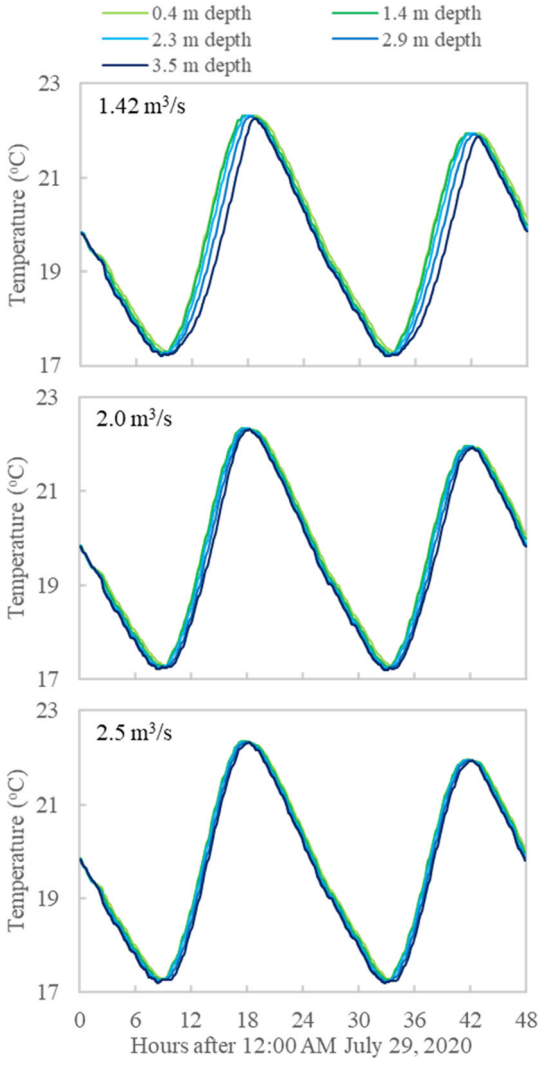

FIGURE 11 Predicted temperatures at the upstream stringer in PT pool

to survive winter (Railsback et al., 2016; Wheeler et al., 2014). Compared to UT pool, the regulated baseflow at PT pool also generates substantially higher velocities that would require a greater expenditure of energy by adult spring Chinook salmon when holding in deep pools in the summer-long period for sexual maturation (Groot & Margolis, 1991). The higher energetic cost may result in lower fitness for gamete production and spawning in fall and possibly detract from their reproductive success (e.g. Mesa & Magie, 2006). Mitigating these impacts by lowering regulated summer baseflows closer to natural levels on the Trinity River could therefore be a prudent step for conservation of these species.

Statistical modelling indicated that discharge and daily air temperature differential had a slightly better AIC score than the model with daily inlet temperature differential and discharge. The difference, however, was small enough that both models are considered competing in performance as best fitting. Numerical modelling did show the daily range in inlet temperatures was the strongest driver of stratification after discharge, while air temperatures appeared to fluctuate with S_d more clearly. However, it is cold nighttime and warm daytime water temperatures at the pool inlet that create conditions necessary for stratification to form and strengthen at sub-critical flows. We also measured critical flows for stratification varied with inlet water temperatures in the diurnal range. This results because density differences in cold (0–10°C) water are small in comparison to higher temperatures, which makes lower flows a requirement for stratifying colder water.

The 3D CFD model U^2RANS closely reproduced temperatures observed during stratification at UT pool and isoclines in PT pool (Lai et al., 2022) and predicted the critical discharge when stratification was first observed at UT pool. The model's strong performance makes it an important new tool for river managers to determine and schedule discharges that meet environmental flow requirements below dams. This can be done by modelling downstream pools to determine critical flows for stratification and then scheduling dam releases above the critical flows to prevent stratification where needed to improve water quality. Alternatively, flows at or below the critical discharge can be released to form stratification and provide temperature diversity that benefits species in rivers. Water saved in the latter approach could then be available for beneficial uses at other times of year. For example, if flows in summer (July–September) were lowered from 12.7 m^3/s at Lewiston Dam to the 2.0 m^3/s flow for stratification at PT pool, ~9.0 × 10^7 m^3 of water would be available to mimic natural flooding for habitat formation at other times of year (e.g. Melis, 2011). Another benefit of a natural as opposed to elevated summer baseflow would be for vegetation to establish lower in the channel where it is more likely to be scoured by floods and contribute organic matter for stream metabolism and river ecosystem health (Young et al., 2008). Plants that survive the scour could then mature and provide flow resistance that promotes sediment deposition and formation of bars and floodplains that are prime habitats for rearing juvenile salmon (Buxton & Bradley, 2022).

Its performance notwithstanding, improvements to the CFD model are possible by addressing the difference between observed and predicted temperatures at the onset of stratification at UT pool (Lai et al., 2022). For example, the thermal diffusivity coefficient in the

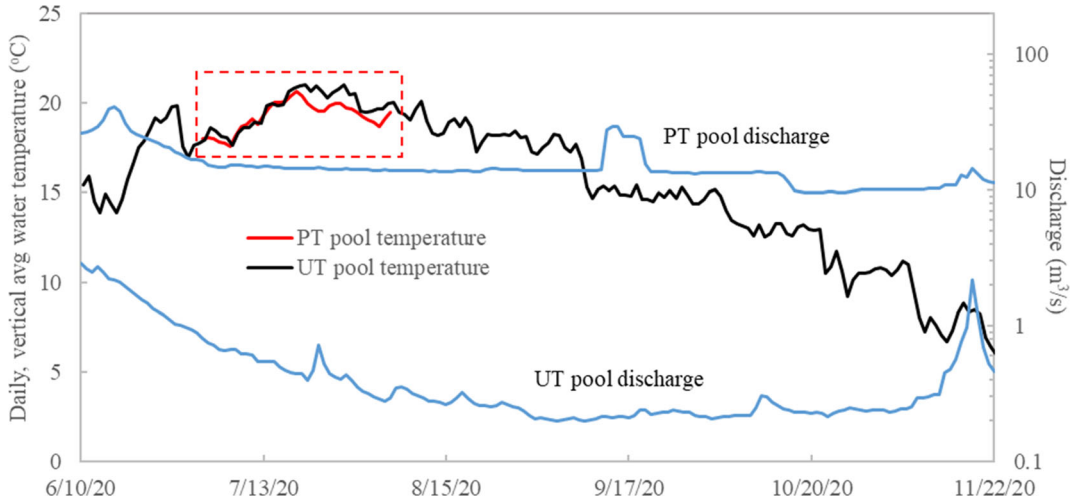

FIGURE 12 Water temperatures averaged in verticals on a daily timestep at UT and PT pool. Dates when stringers were operational at both locations were 1 July through 5 August, 2020. This period includes the highest observed air and water temperatures at both locations.

energy conservation equation could be made a function of the local turbulence and stratification to reflect that the Prandtl number is not actually constant. Another area for potential improvement is the inclusion of the hyporheic flow, which was ignored in the present modelling but might deliver warmer water to the UT pool bottom. This period between 11:00 AM and 5:00 PM is when predicted temperatures were up to 1.8°C lower than temperatures observed in the pool bottom and is within the time lag and temperature deviation that Arrigoni et al. (2008) measured between surface and hyporheic flow in the Umatilla River, Oregon.

Applying the model in a wider range of conditions than done here may expose additional opportunities to improve or better explain model performance through model adjustments or more intensive monitoring at pool sites. Toward this, work is underway to run the model in 14 additional pools between PT pool and Lewiston Dam to estimate stratification flows for a wider range of pool entrance geometries, depths, and sizes than in the current paper. Based on results herein and those of others (Borman & Webster, 1998; Reinfelds & Williams, 2012), we expect that critical flows will scale to pool surface area and provide a first-order estimate of critical flows for stratification. We do not, however, expect that high winds will significantly destabilise stratification, as Borman and Webster (1998) and Turner and Erskine (2005) found, because this effect is probably limited to large pools with surface areas that resemble lakes.

Current trends in climate and estimated impacts to streamflows are foretelling a difficult period ahead for water managers tasked with balancing the water demands of society with flow requirements for rivers and the species that inhabit them. The challenges are highlighted by projections that water availability in summer will lessen, and water temperatures will rise in most salmon-bearing streams. This has raised the possibility that restoration should focus on streams that can provide salmonids refuge to withstand pressures imposed by climate change (Battin et al., 2007; Beechie & 10 co-authors., 2013).

In this sense, our findings are encouraging insofar that stratification at natural baseflows in UT pool provided more temperature diversity with less flow by preserving cold water in the pool bottom and warmer water near the surface than was observed at PT pool. We further discovered that stratification at flows between 0.5 and 1.0 m^3/s at UT pool provided about the same daily and vertically averaged temperature as 14.2 m^3/s at PT pool when stringers were operational in both locations, which included the hottest temperatures in summer (Figure 12). This reveals an opportunity for preserving reservoir storage may lie in releasing closer to natural summer baseflows because they deliver similar overall temperatures in pools and promote thermal diversity that benefits poikilothermic species.

5 | CONCLUSIONS

Diurnal thermal stratification was studied in two deep pools on the Trinity River that receive cold water from surface flow overnight and relatively warm water from solar heating in daytime. The foremost requirement for stratification was an upstream flow that is low enough to prevent temperatures from mixing in the pool. A secondary requirement is for temperatures at the pool inlet to vary so that cold water delivered at night can be preserved by convection in daytime when relatively warm water accesses the pool. Stratification typically forms before mid-day and a slow mixing period ensues as warm surface water transits the pool at the surface and slowly mixes by vertical diffusion with lower depths. In this period, the temperature gradient strengthens as inlet temperatures rise until around late afternoon. Stratification is then rapidly destroyed when inlet water cools below water in top depths of the pool, sinks from its increased density, and collapses the temperature gradient. This returns the pool to a well-mixed state that existed before stratification formed earlier in the day.

The 3D CFD model U^2RANS closely replicated the observed diurnal process of stratification formation and destruction (Lai et al., 2022) and was used to estimate critical discharges for stratification at both pools. The critical discharge modelled at UT pool (1.03 m^3/s) closely agreed with the observed critical flow (1.01 m^3/s).

Stratification was not observed at PT pool because summer baseflows are maintained at an unnaturally high level (14.2 m^3/s) by dam releases. The CFD model predicted isotherms to within 0.25°C of those observed in PT pool and estimated a critical discharge of 2.0 m^3/s at this location. The higher critical flow at PT pool reflects its deep (≥2 m) water being 2.6 times larger in area and width than UT pool, which helps disperse inlet flow velocities and enable stratification at a higher flow. Releasing higher than critical flows can prevent stratification where needed to improve water quality. Lowering regulated summer baseflows to or below the critical flow can promote thermal stratification in pools and provide water temperatures that poikilothermic species use to regulate body temperature. The lower discharges can result in water savings for temperature management in reservoirs, high flow releases for habitat creation at other times of year, and flow releases in emergencies to avoid climate-driven bottlenecks to salmonids under a warming climate.

ACKNOWLEDGEMENTS

The authors thank Ken Lindke, Kevin Held, Kyle DeJuilio, Oliver Rogers, Brandt Gutermuth, Chris Lasdoki, James Lee, and John Guczek for assistance in the field and Jeanne McSloy for help with the elevation surveys and developing several of the figures. This paper benefitted from insightful comments provided by two anonymous reviewers. The U.S. Bureau of Reclamation provided funding to the Trinity River Restoration Program for this study.

DATA AVAILABILITY STATEMENT

The data that support the findings of this study are available from the corresponding author upon reasonable request.

ORCID

Todd H. Buxton https://orcid.org/0000-0003-4131-1588

REFERENCES

Arrigoni, A. S., Poole, G. C., Mertes, L. A. K., O'Daniel, S. J., Woessner, W. W., & Thomas, S. A. (2008). Buffered, lagged, or cooled? Disentangling hyporheic influences on temperature cycles in stream channels. *Water Resources Research*, *44*, W09418. https://doi.org/10.1029/2007WR006480

ASPRS (American Society for Photogrammetry and Remote Sensing). (2014). Photogrammetric Engineering and Remote Sensing. In *ASPRS Positional Accuracy Standards for Digital Geospatial Data* (1st ed., Vol. 81, pp. A1–A26.) version 1.0. American Society for Photogrammetry and Remote Sensing. https://doi.org/10.14358/PERS.81.3.A1-A26

Battin, J., Wiley, M. W., Ruckelshaus, M. H., Palmer, R. N., Korb, E., Bartz, K. K., & Imaki, H. (2007). Projected impacts of climate change on salmon habitat restoration. *Proceedings of the National Academy of Sciences*, *104*, 6720–6725. https://doi.org/10.1073/pnas.0701685104

Beechie, T., Imaki, H., Greene, J., Wade, A., Wu, H., Pess, G., Roni, P., Kimball, J., Stanford, J., Kiffney, P., & Mantua, N. (2013). Restoring salmon habitat for a changing climate. *River Research and Applications*, *29*, 939–960. https://doi.org/10.1002/rra.2590

Bilby, R. E. (1984). Characteristics and frequency of cool-water areas in a western Washington stream. *Journal of Freshwater Ecology*, *2*, 593–602. https://doi.org/10.1080/02705060.1984.9664642

Boles, G. L. (1990). Food habits of juvenile wilds and hatchery steelhead trout, Oncorhynchus, mykiss, in the Trinity River, California. CDFG inland fisheries administrative report 90–10.

Borman, M., & Webster, I. T. (1998). Dynamics of temperature stratification in lowland rivers. *Journal of Hydraulic Engineering*, *124*, 1059–1063. https://doi.org/10.1061/(ASCE)0733-9429(1998)124:10(1059)

Butler, N. L. (2013). Thermal conditions in riverine pools from the eastside bypass/reach 4 to reach 5. Project report, U.S. Department of Interior, Bureau of Reclamation, San Joaquin River restoration program, Sacramento, CA 95825.

Buxton, T. H., & Bradley, D. N. (2022). Evolution of tributary junctions and their capacity for rearing juvenile Chinook salmon (*Oncorhynchus tshawytscha*) on a regulated river. *Ecohydrology*, 2022;e2463. 10.1002.eco.2463

Chatfield, C. (2003). *The analysis of time series: An introduction* (Sixth ed.). Chapman and Hall/CRC. https://doi.org/10.4324/9780203491683

Coates, M. G., & Mondon, J. (2009). Effect of environmental flows on deep, anoxic pools. *Ecological Modelling*, *220*, 1643–1651. https://doi.org/10.1016/j.ecolmodel.2009.03.009

Groot, C., & Margolis, L. (1991). *Pacific salmon life histories*. University of British Columbia Press.

Jesson, M., Sterling, M., & Bridgeman, J. (2013). Despiking velocity time-series–optimization through the combination for spike detection and replacement methods. *Flow Measurement and Instrumentation*, *30*, 45–51. https://doi.org/10.1016/j.flowmeasinst.2013.01.007

Keller, E. A., Hofstra, T. D., & Moses, C. (1990). Geomorphic processes and aquatic in the Redwood Creek basin. In *Summer cold pools in Redwood Creek near Orick, California, and their relation to anadromous fish habitat* (p. 1454). U.S. Geological Survey Prof. Paper.

Lai, Y. G. (2022). Flow characteristics at a river diversion juncture and implications for juvenile salmon entrainment. *Fluids*, *7*, 98. https://doi.org/10.3390/fluids7030098

Lai, Y. G., Buxton, T. H., & Abban, B. (2022). Adaptive planning and Design in an age of risk and uncertainty. In J. Pierson & E. Grubert (Eds.), *3D CFD modeling of river pool stratification characteristics*. World Environmental & Water Resources Congress, June 5–8, 2022. https://doi.org/10.1061/9780784484258

Lai, Y. G., Smith, D. L., Bandrowski, D. J., Xu, Y., Woodley, C. M., & Schnell, K. (2021). Development of a CFD model and procedure for flows through in-stream structures. *Journal of Applied Water Engineering and Research*, *10*, 197–211. https://doi.org/10.1080/23249676.2021.1964388

Lai, Y. G., Weber, L. J., & Patel, V. C. (2003). Non-hydrostatic three-dimensional method for hydraulic flow simulation - part I: Formulation and verification. *Journal of Hydraulic Engineering*, *129*, 196–205. https://doi.org/10.1061/(ASCE)0733-9429(2003)129:3(196)

Lusardi, R. A., Hammock, B. G., Jeffres, C. A., Dahlgren, R. A., & Kiernan, J. D. (2019). Over summer growth and survival of juvenile coho salmon (*Oncorhynchus kisutch*) across a natural gradient of stream water temperature and prey availability: And in situ enclosure experiment. *Canadian Journal of Fisheries and Aquatic Sciences*, *77*, 413–424. https://doi.org/10.1139/cjfas-2018-0484

Marzadri, A., Tonina, D., McKean, J. A., & Tiedemann, M. (2012). Proceedings of the 9th international symposium on Ecohydraulics. In H. Mader & J. Kraml (Eds.), September 17–21, 2012 *Hyporheic exchange along a river below a dam*. Vienna.

Matthews, K. R., Berg, N. G., Azuma, D. L., & Lambert, T. R. (1994). Cool water formation and trout habitat in a deep pool in the Sierra Nevada, California. *Transactions of the American Fisheries Society*, *123*, 549–564. https://doi.org/10.1577/1548-8659(1994)123<0549:CWFATH>2.3.CO;2

Melis, T. S. (2011). Effects of three high-flow experiments on the Colorado River ecosystem downstream from Glen canyon dam, Arizona. *U.S. Geological Survey Circular*, *1366*, 147.

Mesa, M. G., & Magie, C. D. (2006). Evaluation of energy expenditure in adult spring Chinook salmon migrating upstream in the Columbia River basin: An assessment based on sequential proximate analysis. *River Research and Applications*, *22*, 1085–1095. https://doi.org/10.1002/rra.955

Metcalfe, N. B., Fraser, N. H. C., & Burns, M. D. (1999). Food availability and the nocturnal vs. diurnal foraging trade-off in juvenile salmon.

Journal of Animal Ecology, *68*, 371–381. https://doi.org/10.1046/j.1365-2656.1999.00289.x

Nielsen, J. L., Lisle, T. E., & Ozaki, V. (1994). Thermally stratified pools and their use by steelhead in northern California streams. *Transactions of the American Fisheries Society*, *123*, 613–626. https://doi.org/10.1577/1548-8659(1994)123<0613:TSPATU>2.3.CO;2

Pinheiro, J., Bates, D., DebRoy, S., & Sarkar, D. (2021). R Core team. Nlme: Linear and nonlinear mixed effects models. R package version 3.1-152. https://CRAN.R-project.org/package=nlme

Plumb, J. M., & Moffitt, C. M. (2015). Re-estimating temperature-dependent consumption parameters in bioenergetics models for juvenile Chinook salmon. *Transactions of the American Fisheries Society*, *144*, 323–330. https://doi.org/10.1080/00028487.2014.986336

Pryor, C. (2017). 2016 Trinity River focal reach survey report. http://www.trrp.net/library/document?id=2389

R Core Team. (2021). *R: A language and environment for statistical computing*. R Foundation for Statistical Computing. https://www.R-project.org/

Railsback, S. F., Harvey, B. C., Kupferberg, S. J., Lang, M. M., McBain, S., & Welsh, H. H. J. (2016). Modeling potential river management conflicts between frogs and salmonids. *Canadian Journal of Fisheries and Aquatic Sciences*, *73*, 773–784. https://doi.org/10.1139/cjfas-2015-0267

Reinfelds, I., & Williams, S. (2012). Threshold flows for the breakdown of seasonally persistent thermal stratification: Shoalhaven River below Tallowa dam, New South Wales, Australia. *River Research and Applications*, *28*, 893–907. https://doi.org/10.1002/rra.1485

Sauter, S. T., McMillan, J., & Dunham, J. (2001). Salmonid behaviour and water temperature. EPA region 10 temperature water quality criteria guidance development project EPA-910-D-01-001.

Sherman, B. S., Webster, I. T., Jones, G. J., & Oliver, R. L. (1998). Transitions between *Aulacoseira* and *anabaena* dominance in a turbid river weir pool. *Limnology and Oceanography*, *43*, 1902–1915. https://doi.org/10.4319/lo.1998.43.8.1902

Snover, M. L., Adams, M. J., Ashton, D. T., Bettaso, J. B., & Welsh, H. H. (2015). Evidence of counter-gradient growth in western pond turtles (*Actinemys marmorata*) across thermal gradients. *Freshwater Biology*, *60*, 1944–1963. https://doi.org/10.1111/fwb.12623

Swales, S. (1989). The use of instream habitat improvement methodology in mitigating the adverse effects of river regulation on fisheries. In J. A. Gore & G. E. Petts (Eds.), *Alternatives in Regulated River management*. CRC Press.

Sweeney, G. W., & Vannote, R. L. (1984). Influence of food quality and temperature on life history characteristics of the parthenogenetic mayfly, *Cloeon triangulifer*. *Freshwater Biology*, *14*, 621–630. https://doi.org/10.1111/j.1365-2427.1984.tb00181.x

Turner, L., & Erskine, W. D. (2005). Variability in the development, persistence and breakdown of thermal, oxygen and salt stratification on regulated rivers of southeastern Australia. *River Research and Applications*, *21*, 151–168. https://doi.org/10.1002/rra.838

USFWS (U.S. Fish and Wildlife Service) and HVT (Hoopa Valley Tribe) (1999). A report to the secretary, U.S. Department of the Interior. In *Trinity River flow evaluation study, final report*. USFWS, Arcata Fish and Wildlife Office. https://www.trrp.net/library/document?id=226

Wheeler, C. A., Bettaso, J. B., Ashton, D. T., & Welsh, H. H. (2014). Effects of water temperature on breeding phenology, growth, and metamorphosis of foothill yellow-legged frogs (*Rana Boylii*): A case study of the regulated mainstem and unregulated tributaries of California's Trinity River. *River Research and Applications*, *31*, 1276–1286. https://doi.org/10.1002/rra.2820

Woodson, L. E., Wells, B. K., Weber, P. K., MacFarlane, R. B., Whitman, G. E., & Johnson, R. C. (2013). Size, growth, and origin-dependent mortality of juvenile Chinook salmon *Oncorhynchus tshawytscha* during early ocean residence. *Marine Ecology Progress Series*, *487*, 163–175. https://doi.org/10.3354/meps10353

Young, R. G., Matthaei, C. D., & Townsend, C. R. (2008). Organic matter breakdown and ecosystem metabolism: Functional indicators for assessing river ecosystem health. *Journal of the North American Benthological Society*, *27*, 605–625. https://doi.org/10.1899/07-121.1

SUPPORTING INFORMATION

Additional supporting information can be found online in the Supporting Information section at the end of this article.

How to cite this article: Buxton, T. H., Lai, Y. G., Som, N. A., Peterson, E., & Abban, B. (2022). The mechanics of diurnal thermal stratification in river pools: Implications for water management and species conservation. *Hydrological Processes*, *36*(11), e14749. https://doi.org/10.1002/hyp.14749